Nour Noaman[1]
Prabhodh S. Abbineni[2]
Michael Withers[1]
Jens R. Coorssen[3] (ID)

[1]Department of Molecular Physiology, and the WSU Molecular Medicine Research Group, School of Medicine, Western Sydney University, Campbelltown, New South Wales, Australia
[2]Department of Pharmacology, University of Michigan Medical School, Ann Arbor, MI, USA
[3]Departments of Health Sciences and Biological Sciences, Brock University, St Catharines, Ontario, Canada

Research Article

Coomassie staining provides routine (sub)femtomole in-gel detection of intact proteoforms: Expanding opportunities for genuine Top-down Proteomics

Modified colloidal Coomassie Brilliant Blue (cCBB) staining utilising a novel destain protocol and near-infrared fluorescence detection (nIRFD) rivals the in-gel protein detection sensitivity (DS) of SYPRO Ruby. However, established DS estimates are likely inaccurate in terms of 2DE-resolved proteoform 'spots' since DS is routinely measured from comparatively diffuse protein 'bands' following wide-well 1DE. Here, cCBB DS for 2DE-based proteomics was more accurately determined using narrow-well 1DE. As precise estimates of protein standard monomer concentrations are essential for accurate quantitation, coupling UV absorbance with gel-based purity assessments is described. Further, as cCBB is compatible with both nIRFD and densitometry, the impacts of imaging method (and image resolution) on DS were assessed. Narrow-well 1DE enabled more accurate quantitation of cCBB DS for 2DE, achieving (sub)femtomole DS with either nIRFD or densitometry. While densitometry offers comparative simplicity and affordability, nIRFD has the unique potential for enhanced DS with Deep Imaging. Higher-resolution nIRFD also improved analysis of a 2DE-resolved proteome, surpassing the DS of standard nIRFD and densitometry, with nIRFD Deep Imaging further maximising proteome coverage. cCBB DS for intact proteins rivals that of mass spectrometry (MS) for peptides in complex mixtures, reaffirming that 2DE-MS currently provides the most routine, broadly applicable, robust, and information-rich Top-down approach to Discovery Proteomics.

📟 Additional supporting information may be found in the online version of this article at the publisher's web-site

Correspondence: Prof. Jens R. Coorssen, Departments of Health Sciences and Biological Sciences, Brock University, St Catharines, Ontario, Canada
E-mail: jcoorssen@brocku.ca

Abbreviations: 1DE, One-dimensional gel electrophoresis; **AU**, Arbitrary units; **BCA**, Bovine carbonic anhydrase; **BGAL**, β-galactosidase; **CEL**, Chicken egg lysozyme; **cCBB**, Colloidal Coomassie Brilliant Blue; **DS**, Detection sensitivity; **ddH2O**, Double-glass distilled water; **IMPS**, Integrated measure of practical sensitivity; **LDR**, Linear dynamic range; **LLD**, Lowest limit of detection; **LPS**, Lowest practical sensitivity; **MP**, Megapixel; **MW**, Molecular weight; **nIRFD**, Near-infrared fluorescence detection; **PHOSB**, Phosphorylase B; **PI**, Protease inhibitor cocktail; **RT**, Room temperature; **S/N**, Signal-to-noise ratio; **SR**, SYPRO Ruby; **TBP**, Tributylphosphine; **TP**, Tray Position

1 Introduction

Routine, quantitative, Top-down proteomic analyses are effectively carried out using gel-based techniques that resolve protein species from complex mixtures prior to identification via mass spectrometry (MS). In light of continued efforts to fully address limitations, two-dimensional gel electrophoresis (2DE) continues to offer the highest proteome resolution and information content with respect to intact proteoforms in a single, reproducible assay, enabling comprehensive analysis of biological samples at a level necessary for differentially profiling tissues, dissecting molecular mechanisms, and identifying protein biomarkers [1–12]. However, the information that can be extracted from a resolved proteome remains largely limited by the sensitivity of subsequent in-gel protein detection methods [4, 13, 14], and proteins in lowest abundance, which may be central to (patho)physiological processes, likely remain largely undetected and thus unexamined in routine

analyses. Improving the sensitivity of a given detection method is a crucial and ongoing challenge, and while this has been substantially optimised for Western blotting and other targeted approaches [18,20], high in-gel protein detection sensitivity (DS) for Discovery Proteomics has lagged somewhat behind.

In-gel protein staining is the most widely utilised technique for detection of resolved proteins prior to further analysis, with Coomassie Brilliant Blue (CBB) being the most commonly utilised quantitative total protein stain. The use of CBB has been entrenched in gel-based proteomics since Neuhoff and colleagues developed a colloidal CBB (cCBB) formulation that minimised non-specific gel matrix staining. This improved the lowest limit of detection (LLD) for BSA from 1–0.2 μg to 1–0.1 ng (depending on gel thickness) [21, 22], though many groups note an LLD of 30–4 ng across a broader range of protein standards [14, 23–28]. Indeed, relative to currently available fluorescent stains such as SYPRO Ruby (SR), and densitometric stains such as silver, cCBB as a densitometric stain is generally perceived as lacking adequate DS for thorough proteome analysis due to higher LLD and limited linear dynamic range (LDR) [16, 25, 29–33]. The continued widespread use of cCBB over many alternative technologies is thus largely attributed to its many redeeming features including ease of use, low cost, quantitative capacity, 'reasonable' sensitivity, and compatibility with MS.

Over a decade ago, in a comprehensive review of fluorescent technologies for 2DE-based proteomics, Patton remarked, "a stain that can be considered conceptually as a fluorescent CBB stain offers the broadest applicability" [34]. Fortuitously, several years later, it was found that CBB exhibits fluorescence in the near-infrared when bound to protein [16, 19]. This led to further studies into the use of cCBB staining coupled with near-infrared fluorescence detection (nIRFD) for the in-gel assessment of resolved proteins. More recent studies have concluded that the DS of cCBB rivals that of SR when using the original Neuhoff cCBB stain formulation, or a variant with slightly higher dye content, coupled with a novel NaCl destain protocol and nIRFD. Not only was cCBB LLD shown to be comparable to that of SR, but measures of many other DS parameters, including LDR, were equivalent or better [3, 13, 18, 35].

Assessments of stain DS generally utilise protein standards resolved via SDS-PAGE (1DE) as 2DE models from which DS parameters are measured (e.g. LLD, LDR, interprotein staining variability (IPV), and signal-to-noise ratio (S/N)). However, factors outside of stain performance *per se*, including the purity and concentration of protein standards, as well as resolving method, imaging instrumentation, and image resolution, all likely influence 1DE-based measures of DS [35]. Here we have examined these factors and optimised as feasible in order to accurately determine the DS of the modified cCBB staining protocol for application in 2DE-based Discovery Proteomics.

Rather than be taken at face-value as seems often the case in the literature, manufacturer-specified purity and concentration of protein standards must be independently assessed in order to accurately quantify the DS of a given stain. Having more or less of a protein standard (i.e. the pure, monomeric protein) leads to inaccurate determinations of DS, and impurities may further distort measures of concentration and thus quantitative assessments, particularly if standards are combined into single cocktails in which contaminants may co-migrate with target proteins. Here, the purity and concentrations of commercial protein standards were thoroughly characterised by combining two approaches – UV absorption and gel-based analysis (coupled with MS)– to accurately quantify DS.

A drawback of 1DE models is that resolved proteins form relatively diffuse 'bands' as opposed to concentrated 2DE 'spots', likely significantly lowering S/N and leading to inaccurate determinations of DS for application to 2DE. Here, relatively narrow loading wells than typically utilised for such studies were used to concentrate 1DE-resolved protein bands to better represent concentrated 2DE-resolved protein spots, thus enabling improved and more accurate measures of cCBB DS relevant to 2DE.

Following protein resolution and staining, gels are imaged to enable subsequent quantitative analyses, necessitating that the acquired digitised data accurately represent the analogue data (i.e. the stained gel) in as much detail as possible. Accordingly, imaging method can impact analytical outcomes. A previous report comparing densitometry with nIRFD for the detection of a cCBB-stained proteome following 2DE showed that densitometry provided approximately half the DS of nIRFD [14]. However, a less sensitive commercial cCBB formulation had been utilised [8], and unspecified imaging parameters (exposure, extent of data 'binning') may have been sub-optimal. Thus, the poor DS may have been due to a combination of factors rather than being inherent to densitometric detection. With the advent of higher calibre instrumentation for densitometry, potentially capable of higher DS (e.g. lower noise, higher resolution), as well as the novel NaCl destain protocol which further improves cCBB-nIRFD DS [13], reassessment of cCBB DS with densitometric detection is appealing due to generally greater simplicity and cost-effectiveness of such instruments (i.e. specialised filters and/or lasers are unnecessary). Here, the performance of nIRFD (via laser scanning) was compared against that of premium instrumentation for densitometry (using a camera-based system) for detection of (i) protein standards following 1DE, and (ii) protein standards and a native proteome following 2DE. As the capacity of both instruments for high-resolution imaging could also further improve DS, the impact of image resolution on DS was also assessed.

Overall, the data indicate that proteins resolved via narrow-well 1DE models more closely resembled 2DE-resolved proteins, delivering more accurate, (sub)femtomole DS assessments, confirmed following 2DE of protein standards. Furthermore, densitometric detection provided competitive DS relative to standard resolution (100 μm) nIRFD for 2DE-resolved proteome detection, and higher resolution (50 μm) nIRFD significantly improved 2DE analysis,

increasing the quality and quantity of protein spots detected – further still with nIRFD Deep Imaging.

2 Materials and methods

All consumables were of electrophoresis grade or higher. Broad-range (7 cm, pH 3–10 non-linear) ReadyStrip™ IPG Strips, Bio-Lyte® carrier ampholyte solutions (pH 3–10; 3–5; 6–8; 7–9; and 8–10), Precision Plus Protein™ Unstained Standards, and tributylphosphine (TBP) were supplied by Bio-Rad Laboratories (Hercules, CA). Isolated protein standards (β-galactosidase from *E. coli* (BGAL); Phosphorylase B from rabbit muscle (PHOSB); Bovine Serum Albumin (BSA); Bovine Carbonic Anhydrase (BCA); and Chicken Egg Lysozyme (CEL)) (Supplementary Table 1), kinase and phosphatase inhibitors (staurosporine, sodium orthovanadate, and sodium fluoride), and components of the protease inhibitor cocktail (PI) [36] were supplied by Sigma-Aldrich (St. Louis, MO). Invitrogen (Carlsbad, CA) supplied the EZQ Protein Quantitation Kit, and all other consumables for electrophoresis and stain preparation, including CBB G-250 dye, and acrylamide/bis-acrylamide (37.5:1) solution, were supplied by Amresco (Solon, OH). Double glass-distilled water (ddH$_2$O) was used throughout.

2.1 Sample preparation

Isolated protein standards (BGAL, PHOSB, BSA, BCA, and CEL) were each solubilised in ddH$_2$O and centrifuged at 2000 × g for 5 min at room temperature (RT, 21°C) to remove insoluble particulates [13]. Concentrations and purities were assessed as detailed in Section 2.2 prior to snap-freezing of aliquots and storage at −80°C until required. Prior to SDS-PAGE, aliquots were thawed (once only) and serially diluted in 1DE sample buffer (25 mM TRIS [pH 8.8], 12.5 mM DTT, 7.5% (w/v) glycerol, 2% (w/v) SDS, and 0.001% (w/v) bromophenol blue [13,37,38]) to yield 1.6-0.006 µg/mL solutions for 8–0.03 ng protein loads for 1DE DS estimates.

For native proteome 2DE, rat cortex soluble proteome was extracted as previously described and supplemented with kinase and phosphatase inhibitors and PI [1,2]. Total protein concentration was estimated using the EZQ Protein Quantitation Kit (Invitrogen, Carlsbad, CA). Snap-frozen aliquots were stored at -80°C until required.

2.2 Protein standard concentration and purity assessments

Initial measures of protein standard concentrations were according to the Beer–Lambert law [13, 18, 39]. For each, path length-corrected absorbance (A$_{280}$) was measured in a quartz cuvette using the UV-2550 Shimadzu UV-VIS Spectrophotometer (Shimadzu, Tokyo, Japan). Theoretical

percent-solution extinction coefficients were obtained from ExPASy ProtParam (http://web.expasy.org/protparam/).

Gel-based purity analysis was essentially as described [15, 18]. Based on UV-absorption concentration estimates, each protein standard was serially diluted to yield 1–0.0625 mg/mL solutions in 1DE sample buffer for 10–0.625 µg protein loads. SDS-PAGE was carried out as described in Section 2.3 using 7–20%T gradient gels for MS analysis of resolved proteins, and 12.5%T uniform gels to measure percentage purity of target monomer protein bands.

From gradient gels, following cCBB staining as detailed in Section 2.4, all well-resolved bands were excised and processed for LC-MS/MS analysis as described previously [4, 13]. Following database (Swiss-Prot) confirmation of protein identifications via Mascot Daemon (version 2.2.2) (www.matrixscience.com), it was apparent that 'contaminants' were predominately multimers and/or degradation products of corresponding protein standards. To account for these 'impurities', measured from uniform %T purity gels, target protein monomer band signal was expressed as a percentage of total lane signal (using Multi Gauge v3.0 (FUJI-FILM, Tokyo, Japan)) from the lowest protein load in which all contaminating bands could be detected [18]. For each protein standard, initial protein concentration estimates were adjusted based on the percentage of the total lane signal that corresponded to the monomer band. To ensure there was no further formation/degradation of multimers due to freeze/thawing of standards (i.e. that target band percentage remained stable and reproducible), gel-based purity analysis using uniform %T gels was routinely carried out in parallel with gels for 1DE DS analysis.

2.3 IEF and SDS-PAGE

Passive rehydration of IPG strips and subsequent IEF was as described [1, 2, 16, 40, 41]. IPG strips were rehydrated for 16 hrs at RT with 100 µg of soluble protein from rat cortex in 2DE buffer (8 M urea, 2 M thiourea, and 4% (w/v) CHAPS) supplemented with PI and 1% (v/v) carrier ampholytes (0.5% (v/v) pH 3–10, and 0.25% (v/v) each of pH 3–5, 6–8, and 8–10). Reduction and alkylation were carried out at 25°C prior to rehydration, with the addition of 45 mM/2.3 mM DTT/TBP in the first hour followed by 230 mM acrylamide in the subsequent hour [2, 41]. IEF using the Protean IEF system (Bio-Rad Laboratories, Hercules, CA) was carried out at 17°C [41]. Immediately prior to SDS-PAGE, strips were equilibrated in 6 M urea, 20% (w/v) glycerol, 2% (w/v) SDS, and 375 mM Tris (pH 8.8), supplemented first with 2% (w/v) DTT for 10 min, then with 350 mM acrylamide for a further 10 min [2].

SDS-PAGE was according to Laemmli [38] with minor modifications [18, 37]. Using the MiniProtean II system (Bio-Rad Laboratories, Hercules, CA), resolving gels were cast and stored overnight at 4°C following polymerisation at RT. Resolving gels were 82 mm x ~58 mm x 1 mm. For 1DE DS analysis, commercially sourced combs with 5 mm

(wide/standard) and 2 mm (narrow) teeth were used to cast loading wells in 5%T stacking gel, overlayed onto 12%T resolving gel. Samples in 1DE buffer were vortexed thoroughly, heated for 7 min at 100°C, sonicated for 5 min, and cooled to RT prior to loading. For 2DE, molecular weight marker (blotted onto filter paper) and equilibrated IPG strips were overlayed onto 5%T stacking gel and embedded in 0.5% (w/v) low-melting agarose prior to SDS-PAGE in 12.5%T resolving gels.

Electrophoresis was carried out in a cold room (4°C) at constant voltage. 150 V were applied until samples entered the stacking gel (5 min), followed by 90 V until completion [2, 13, 18]. Fixation was in 10% (v/v) methanol and 7% (v/v) acetic acid for 1 hr (minimum) at RT with gentle rocking (60 rpm), and gels were washed 3 x 20 min with ddH$_2$O prior to staining [2, 13, 40].

2.4 Staining

Gel staining was according to Neuhoff et al, [21, 22] with modifications described by Gauci et al, [13]. Staining solution, made fresh immediately prior to use, consisted of 2% (v/v) phosphoric acid, 10% (w/v) ammonium sulfate, 0.1% (w/v) CBB, and 20% (v/v) methanol, made to volume with ddH$_2$O, combined in this order with thorough mixing after each addition. Stain was applied immediately following preparation, and gels were incubated for 20 hrs at RT with gentle rocking. Following staining, gels were washed 5 x 15 min with 0.5 M NaCl and stored overnight in 20% (w/v) ammonium sulfate prior to imaging [13, 21, 22].

2.5 Imaging

All gels were imaged individually. Purity analysis gels were imaged by nIRFD using the Typhoon™ FLA 9000 (GE Healthcare, Buckinghamshire, UK). All other gels (1DE and 2DE) were imaged by nIRFD, as well as densitometry using white light trans-illumination on the ImageQuant™ LAS 4000 Biomolecular Imager (GE Healthcare, Buckinghamshire, UK) equipped with a 3.2 MP (11 μm pixels) charge-coupled device (CCD).

Densitometry images were captured using 'high resolution' sensitivity and 5 sec (optimal; not shown) 'precision' exposure, at tray positions (TP) 1 – 4, yielding 37, 49, 61, and 72 μm pixel sizes, respectively. For simplicity, DS at TP1 and TP2 (37 and 49 μm pixels, respectively) are shown for 1DE, and DS at TP1 and TP4 (37 and 72 μm pixels, respectively) are shown for 2DE.

For nIRFD, gels were imaged using 685 nm laser excitation and ≥750 nm emission [13, 16]. 1DE and 2DE DS analysis gels were imaged with scanning pixel size set to 100 μm (the standard resolution utilised for CBB-nIRFD [3, 13]), 50 μm (higher resolution), and 200 μm (lower resolution). Unless stated otherwise, PMT gain was set to 600 V (the standard PMT setting for CBB-nIRFD [3, 13]), though 750 V PMT was also assessed for increased sensitivity [3, 4]. Prior to imaging,

1 mL of ddH$_2$O was applied and spread across the gel surface, and gel edges were lined with ddH$_2$O to prevent dehydration and distortions caused by overheating during extended laser imaging.

Following whole-gel (i.e. first-pass) imaging, Deep Imaging was carried out on narrow-well 1DE as well as 2DE gels [3, 4]. Comparatively 'saturated' gel regions were excised prior to imaging again with all nIRFD settings detailed above. From 2DE gels, protein spots contributing to the top 20% of total signal (determined using Multi Gauge) were excised, whereas the 8 and 4 ng protein bands were excised from 1DE gels, with molecular weight marker and dye fronts removed in all cases.

2.6 1DE analysis

All 1DE gel images (16-bit IMG (raw) files) were analysed using Multi Gauge v3.0 (FUJIFILM, Tokyo, Japan). For 1DE DS assessments, visible target protein bands were delineated using the 'magic wand' tool, and the smallest sized region of interest was copied to the locations of bands that were visually undetectable by systematically tracking their position based on the spacing and positions of visible bands. Per band, two background measurements were taken from immediately adjacent, protein-free regions of the gel. Resulting raw data were analysed in Microsoft Office Excel to establish values for the detection criteria defined below.

LLD: Signal from all measured regions, quantified as volumes (the sum of the pixel volumes within the specified areas) in arbitrary units (AU), were normalised to yield signal/mm^2. Average local background signal was subtracted from corresponding protein signal, and linear standard curves were generated using data points for 2–0.06 ng of protein (except for PHOSB, for which signal for 8–1 ng of protein was plotted). For each replicate, LLD was calculated using standard linear regression, defined as the amount of protein signal equal to three standard deviations from the mean signal of all background measurements [13, 15, 42]. Average LLDs are reported.

IMPS: To better gauge the DS of each assessed condition, IPV was also considered by integrating two measures of DS – LLD and lowest practical sensitivity (LPS) – to obtain the integrated measure of practical sensitivity (IMPS), where IMPS = 1 / (LLD x LPS), and high IMPS values indicate greater DS [15]. LPS was defined as the highest quantity of protein (across all assessed proteins) that exhibited background-subtracted signal that was statistically indistinguishable from background (i.e. equal to one standard deviation from the mean signal of all background measurements [15]). As PHOSB was the most poorly detected protein, all LPS values were derived from PHOSB gels.

S/N: Signal-to-noise ratio (S/N, the ratio of protein signal to local background [16]) was calculated for each detection method, averaged across all assessed proteins, using signal/mm^2 values without background subtraction (i.e. raw target band signal over average local background signal). As

S/N was proportional to protein load, for simplicity, only average S/N for 2 ng protein is reported.

2.7 Image analysis of 2DE-resolved proteomes

Using Multi Gauge, 2DE gel images (16-bit IMG files) were cropped to uniform dimensions and boundaries, excluding marker and dye fronts, and analysed using Delta2D v.4.0.8 (DECODON, Greifswald, Germany).

To compare spot detection (i.e. a measure of 2DE DS) between imaging modes, automated spot detection was carried out on raw unfused images to assess variance, and on warped 'union fusion' images (i.e. weighted average gel images for each condition), without image filtering, to minimise the incidence of artefactual spot detection. No manual editing of spots was performed except for Deep images in which cutting artefacts were excluded, and excised spots were included in the final total spot number. Parameters for spot detection, i.e. average spot size (radius, in pixels) and sensitivity, which enabled maximal spot detection and minimal artefacts/errors (scrutinised by eye) were utilised, and adjusted according to image resolution. Based on automated analysis of a gel region containing largely only distinctly resolved, moderately abundant proteins, average spot size for 100 μm nIRFD images was set to two pixels. Thus, average spot sizes for 50 and 200 μm nIRFD images were adjusted to four and one pixels respectively; and for densitometry images, average spot sizes were adjusted to six, five, four, and three pixels for 37, 49, 61, and 72 μm images, respectively.

2.8 Statistics

Errors are reported as standard deviation from the mean (SD). Statistical analyses were with SigmaPlot (Systat Software, San Jose, CA). To determine the impact of imaging method on 1DE and 2DE (proteome) DS, all conditions assessed were considered discreet treatments, and one-way ANOVA with post-hoc Holm-Šídák pairwise comparisons [43] was carried out. Statistically significant differences from control (i.e. 100 μm 600 V PMT nIRFD, of standard-well models for 1DE, and whole gels for 2DE) are reported, as well as significant differences between the various imaging methods versus 100 μm 600 V PMT nIRFD of narrow-well 1DE models only. Student's unpaired *t*-test was used to determine statistical differences between standard versus narrow-well 1DE outcomes, and whole versus Deep Imaging outcomes for 2DE. *P* values less than 0.05 were considered statistically significant. Refer to figure legends for statistical analyses not detailed here.

2.9 2DE of protein standards

To assess the accuracy of 1DE-derived LLDs for 2DE application – as well as to examine how closely narrow-well 1DE mimicked 2DE gels in terms of concentrating resolved protein – protein standards (BGAL and BCA) were resolved via 2DE as described in Section 2.3. Serially diluted, relatively high loads of each protein (2–0.125 μg of BGAL ($n = 2$) and 2–0.25 μg of BCA ($n = 3$)) were resolved in order to detect and adjust for charge variants, using 10%T gels for second-dimension SDS-PAGE of BGAL. Following cCBB staining and 100 μm nIRFD, Multi Gauge analysis (i.e. manual delineation and subtraction of average local background) was used to quantify the most prominent proteoform at the expected MW and p*I*.

BCA resolved as multiple charge variants at the expected MW (all confirmed as BCA by MS (not shown)), with the most prominent protein spot consistently comprising 30 ± 3% of the combined fluorescence signal. As the relationship between protein quantity and cCBB-protein signal is linear across a broad dynamic range generally irrespective of IPV [13, 15, 19, 44], the protein spot quantified in BCA gels was considered to be 30% of the total BCA monomer content, and subsequent 2DE BCA gels were loaded accordingly. Multiple proteoforms were not discernible following 2DE of 2–0.125 μg of BGAL, so the resulting 'streak' was assessed as a whole and no adjustments to BGAL monomer concentration were made. Briefly, 2DE LLDs extrapolated from microgram-loaded 2DE gels were estimated to be 66 ± 20 ng for BGAL, and 2 ± 2 ng BCA, though since protein spot shape and size following 2DE (i.e. how concentrated the resolved proteoform is), as well as protein load, determines protein spot signal, this approach evidently could not be used to reliably measure 2DE DS.

2DE of nanogram protein loads (160–0.06 ng of BGAL, and 160–0.25 ng of BCA) was then carried out. Note that the higher protein loads (160–40 ng) were routinely included in the same IEF tray as lower protein loads (4–0.06 ng) since IEF of low- and sub-nanogram protein loads alone resulted in poor resolution and detection. Resulting 2DE gels were cCBB-stained and imaged via 100 and 50 μm nIRFD (whole and Deep Imaging, 600 V PMT) and 37 μm densitometry, as described above.

Images were analysed using Delta2D to confirm the accuracy of narrow-well 1DE-derived LLDs for 2DE application, by way of assessing whether these exceptionally low 2DE-resolved protein loads could be detected using the highly automated 2DE analysis software. Per protein load, cropped images were warped and fused, and the target protein spot on the fused image was delineated using the 'spot editing' tool. While the more manual process of spot editing offered some control over how much excess area was included for analysis (i.e. spot boundaries were recalculated until a minimal inclusion area was achieved), which aided in achieving consistency for meaningful comparisons, ultimately, the region analysed was software-determined. The 'consensus spot pattern' (i.e. the single spot delineation) was then transferred to all gel images to obtain absolute spot volumes (grey values; black = 1). Spot volumes for 1–0.06 ng BGAL and 2.4–0.15 ng BCA are reported. Note that fully automated detection of the target protein of all loads assessed, with minimal detection

of weaker 'above background' signal (i.e. any non-protein signal remaining following automated background subtraction), could be achieved by decreasing the sensitivity parameter in Delta2D to 5–8% rather than the recommended 20%.

Multi Gauge image analysis was carried out to compare 1DE band and 2DE spot size and signal, measured from 100 μm nIRFD and 37 μm densitometry images of 1DE and 2DE BCA gels. A comparison of background-subtracted signal/mm^2 from 0.5, 1, and 2 ng BCA is reported.

3 Results and discussion

3.1 An integrated approach for accurate protein quantitation

Accurate assessments of the concentration and purity of protein standards are necessary for meaningful determinations of stain sensitivity and selectivity. Apparent impurity of commercial protein preparations has been seen to varying degrees [19, 25, 28, 45–47], and noted in other investigations in which protein concentration and purity were assessed [13, 15, 18, 48]. Yet it remains a problem in the field that efforts to examine the content/purity of commercial protein standards (and detailing methods to do so) are rarely reported if carried out at all. This signifies a root source of variability both within and between investigations that must be addressed in order to meaningfully measure the DS of any given method.

Protein UV absorbance coupled with the Beer–Lambert law is the method most commonly used to determine the concentration of purified proteins [39]. In this study, concentration determinations with UV absorbance indicated that the assessed standards contained ~99–200% of the protein content claimed by the suppliers (Supplementary Table 1), indicating varying degrees of (im)purity and/or generally greater quantities of protein than specified. The latter is noteworthy and problematic if supplier-indicated protein amounts are taken at face value in stain performance studies, particularly if the protein content of the target band quantified in fact accounts for only a fraction of the total protein loaded.

To validate UV-based protein estimates, i.e. assess sample purity and content, 1DE gel-based analysis was carried out [15, 18], confirming substantial contamination (Supplementary Figure 1A). MS analysis of contaminant bands in each sample confidently identified peptides corresponding only to the expected protein standard (not shown), indicating that these were predominately multimers and/or peptides (i.e. degradation products) of the corresponding protein standards. Indeed, protein spots corresponding to the approximate molecular weights of dimers and tetramers, as well as charge variants, were apparent following 2DE of BCA (Fig. 3A). Thus, while protein standard purity was high, the 'purity' of the target monomer protein band at the expected molecular weight relative to other resolved bands was quite low in most cases, consitituting 37–91% of total lane contents (Supplementary Figure 1B; Supplemenetary Table 1).

Consequently, initial UV absorbance-based concentration estimates were adjusted according to these measures of gel-based purity (Supplementary Table 1) [15, 18]. This approach was highly reproducible, both in terms of monomer band signal between gels, and monomer signal as a percentage of total lane signal (not shown) between initial purity assessment gels and those run in parallel with gels used to determine 1DE DS (Supplementary Fig. 1B), facilitating more accurate quantitation of DS. We thus propose that comparable assessments of purity and concentration should be used and detailed in future studies in order to improve accuracy and minimise variability so as to ultimately establish consistent measures of DS for gel-based proteomics.

3.2 A better 1DE model to assess 2DE DS

DS is often assessed by resolving protein standards via 1DE using ~5 mm wide loading wells. However, as fully resolved protein spots in 2DE gels are more compact and concentrated, such 1DE models cannot provide accurate estimates of DS in terms of 2DE. Here, 2 mm (narrow) loading wells, cast with commercially available narrow-tooth combs, successfully served to concentrate 1DE resolved protein bands to more closely resemble 2DE-resolved proteins in terms of overall area and signal per unit area (Fig. 1A; Fig. 3E).

Qualitative improvements to DS with narrow-well 1DE were generally apparent by eye (Fig. 1A) and were confirmed following quantitative image analysis (Fig. 1B–F; Fig. 2). LLDs with 100 μm nIRFD were improved from (i) 1.33 ± 0.17 ng with standard wells to 0.29 ± 0.06 ng with narrow wells for BGAL; (ii) 15.62 ± 4.52 ng to 3.53 ± 1.42 ng for PHOSB; (iii) 1.05 ± 0.22 ng to 0.40 ± 0.19 ng for BCA; and (iv) from 1.07 ± 0.25 ng to 0.61 ± 0.11 ng for CEL (Fig. 1B, C, E and F). For BSA the difference in LLD fell short of statistical significance, decreasing from 0.60 ± 0.20 ng to 0.35 ± 0.05 ng ($p = 0.057$) with standard versus narrow wells, respectively (Fig. 1D). Overall, LLD with 100 μm nIRFD decreased by ~43–78% with narrow-well 1DE models, with between 50.35 fmol (CEL) and 1.98 fmol (BGAL) detected.

DS following 37 μm densitometry was also significantly increased with narrow-well models, with LLDs decreased by ~58–90%. LLDs improved from (i) 0.39 ± 0.18 ng with standard wells to 0.04 ± 0.03 ng with narrow wells for BGAL; (ii) 5.00 ± 1.96 ng to 2.08 ± 0.74 ng for PHOSB; and (iii) 0.17 ± 0.08 ng to 0.05 ± 0.03 ng for BSA (Fig. 1B–D). Improvements to LLD were not statistically significant for BCA (0.42 ± 0.19 ng to 0.21 ± 0.05 ng; $p = 0.074$) and CEL (0.50 ± 0.16 ng to 0.33 ± 0.10 ng; $p = 0.12$) (Fig. 1E and F). Overall, LLD with densitometry and narrow-well 1DE ranged between 30.07 fmol (CEL) to as low as 0.09 fmol (BGAL).

Regardless of imaging method, IMPS values confirmed that narrow-well 1DE resulted in significantly higher DS compared with standard-well models (Fig. 2A), regardless of the protein assessed. The enhanced DS afforded by narrow-well models is presumably due to greater local 'packing' of protein-CBB complexes, significantly increasing S/N
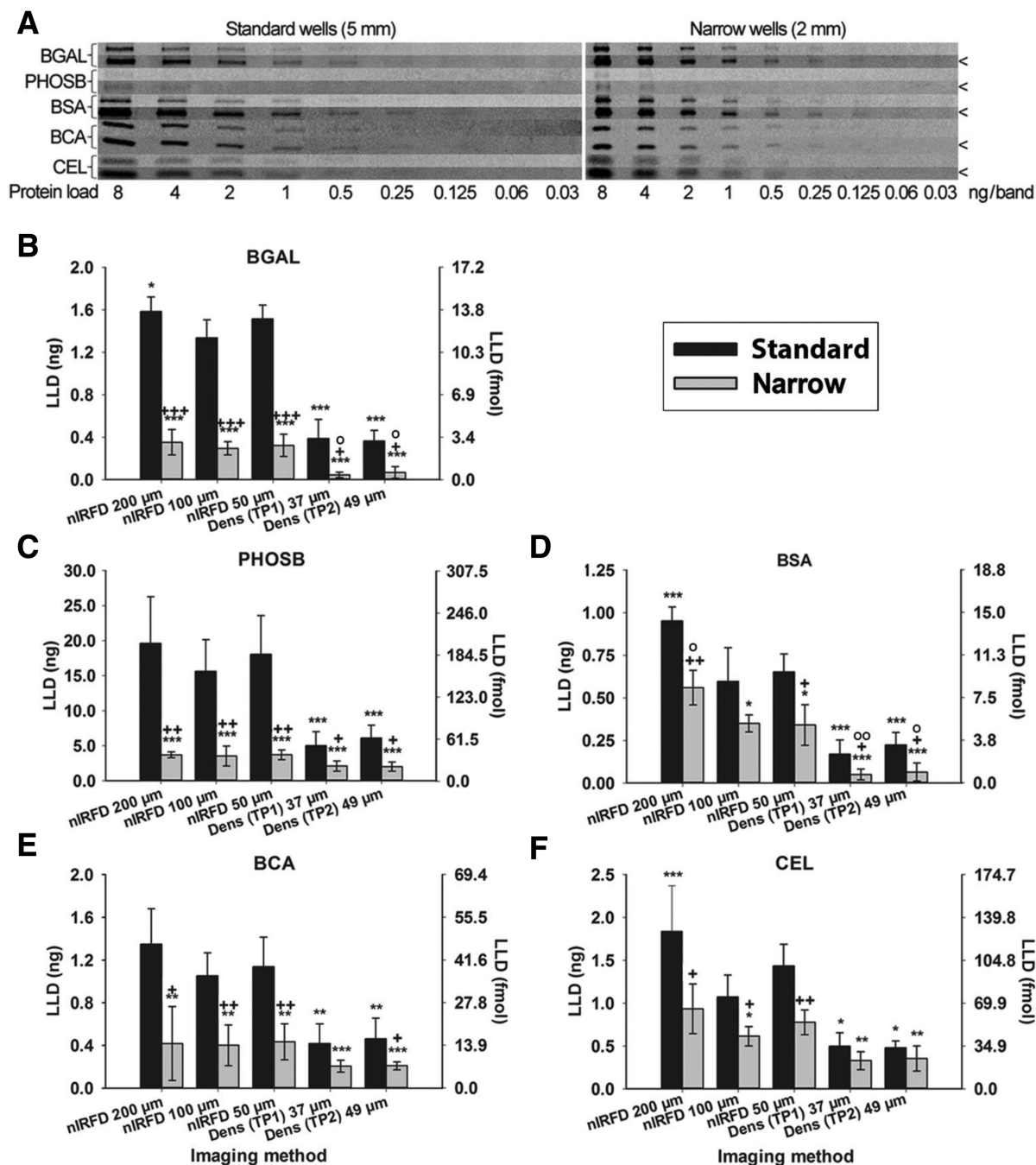
Figure 1. (A) Representative gel images following 1DE of protein standards using standard (5 mm) and narrow (2 mm) loading wells, stained with modified cCBB, and imaged via 100 μm nIRFD and 37 μm densitometry (indicated by '<'). Amounts of protein per load (ng) are indicated. For representative visualisation and comparison, images were contrasted to their maximum and minimum grey values. (B–F) Bar graphs showing cCBB LLD (ng and fmol) with varied imaging methods and well width. Statistically significant differences (Student's *t*-test) from standard versus narrow wells are indicated by '+'. Statistically significant differences (Post-hoc Holm-Šídák test) from standard-well 100 μm nIRFD are indicated by '*', and from narrow-well 100 μm nIRFD are indicated by '°' One symbol indicates $p < 0.05$; two indicates $p < 0.005$; and three indicates $p < 0.001$ (One-way ANOVA, $p < 0.001$; $n = 3$–4).

(Fig. 2B) thereby improving LLD. Interestingly, Neuhoff et al. suggested that dye diffuses in-gel to areas of greater protein concentration (i.e. stain density increases with particle density [49]), thus an additional factor may be that DS was enhanced by recruitment of greater numbers of CBB molecules

per protein following the use of narrow wells to effectively increase the local concentration of resolved proteins.

LLDs derived from narrow-well 1DE models were validated following 2DE of commercial standards (Fig. 3B–D), demonstrating the translatability of these estimates for 2DE
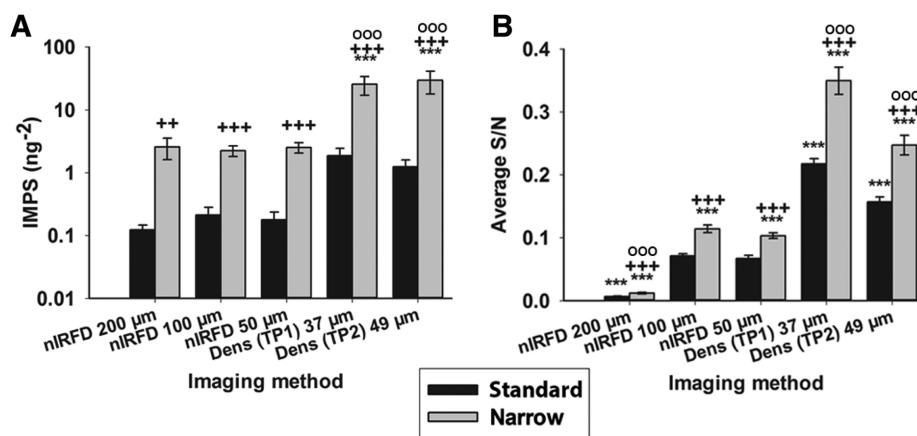
Figure 2. Bar graphs showing (A) IMPS (ng), and (B) average S/N for 2 ng protein with varied imaging methods and well width. Statistically significant differences (Student's *t*-test) from standard versus narrow wells are indicated by '+'. Statistically significant differences (Post-hoc Holm-Šídák test) from standard-well 100 μm nIRFD are indicated by '*', and from narrow-well 100 μm nIRFD are indicated by '°'. One symbol indicates *p* < 0.05; two indicates *p* < 0.005; and three indicates *p* < 0.001 (One-way ANOVA, *p* < 0.001; *n* = 3–4).

application. However, S/N was improved further with 2DE in comparison to narrow-well 1DE, shown by significant increases in background-subtracted protein signal following 2DE of BCA (Fig. 3E). Accordingly, LLDs following 2DE surpassed those estimated from narrow-well 1DE models. While significantly increased S/N following 2DE was most consistently observed with densitometry, the trend was observed with both imaging methods. This increased S/N likely explains how 0.06 ng (0.52 fmol) of BGAL and 0.15 ng (5.17 fmol) of BCA were detected with 100 μm nIRFD following 2DE (Fig. 1B and E; Fig. 3C and D) – substantially less than the amounts detected following nIRFD of narrow-well 1DE models.

Indeed, fully automated detection (i.e. no spot editing) of nanogram protein loads was achieved by adjusting Delta2D analysis parameters (namely, sensitivity) to exclude artefacts, confirming that the signal(s) from resultant protein spots were truly discernible from background and residual noise. Note also that potential protein losses throughout the 2DE protocol have not been considered. It is thus likely that even lower quantities were detected. Certainly, it is evident that narrow-well 1DE DS estimates still did not definitively describe cCBB DS with respect to 2DE. However, the DS estimates reported here are considerably more representative of cCBB DS for 2DE than those derived from wide-well 1DE models [13, 14, 19]. Naturally, this draws into question the accuracy of DS estimates determined for all other stains assessed in the 'conventional' approaches to date.

In terms of more accurately estimating cCBB DS for 2DE from narrow-well 1DE-derived assessments, correction factors of up to ~80 and ~30% would apply following nIRFD and densitometry, respectively, based on the 1DE and 2DE data for BGAL and BCA (Fig. 1B and E; Fig. 3C and D). However, empirical testing of resulting DS estimates must follow. In terms of fully establishing the most simple and direct 1DE method to assess 2DE DS, it may be worthwhile to test still narrower wells (i.e. <2 mm), though this may be impractical. It is thus notable that we did test narrow shark-tooth combs, but the resulting diffuse V-shaped 'band' obviated any effective quantitative analysis (not shown).

3.3 Densitometry offers comparable DS to standard nIRFD

In principle, as laser/PMT imaging systems (used here for nIRFD) generally offer greater S/N compared with CCD/camera systems (used here for densitometry) [50], and largely only protein-bound CBB should fluoresce [16, 19], nIRFD would be expected to have the advantage of innately higher DS compared to densitometry. It was also shown that nIRFD substantially outperformed densitometry following cCBB staining – approximately twofold for 2DE (native proteome) DS in particular [16] – even with nIRFD carried out using a comparatively lower sensitivity instrument than utilised here [13]. However, those findings may have resulted from a combination of factors including staining with a lower sensitivity commercial formulation [13], specifics of instrumentation and imaging parameters, and analysis software employed (Progenesis Workstation 2005, which performs differently to Delta2D [55]), rather than being due to an inherent insensitivity of densitometric detection compared with fluorescence. Certainly, the 1DE and 2DE DS results of this study demonstrate that densitometry matches, and in some regards outperforms, cCBB DS with standard 100 μm nIRFD. However, as discussed further below, densitometry did not enable optimal detection of the 2DE-resolved proteome when coupled with the 2DE analysis software utilised here.

Irrespective of well width, 37 μm densitometry of 1DE gels consistently achieved significantly lower LLD (i.e. improved DS) relative to nIRFD. From narrow-well models, between 40 and 95% less protein was detected with densitometry compared with 100 μm nIRFD (Fig. 1B–F). IMPS and S/N values showed that densitometry provided the highest 1DE DS overall (Fig. 2). LLDs following densitometry of narrow-well models were also more accurate relative to nIRFD in terms of predicting 2DE LLD (Fig. 1B and E; Fig. 3B–D).

Initially, for reasons outlined in Section 3.4, we suspected that the high 1DE DS with densitometry resulted from the comparatively high image resolution (100 versus 37 μm pixels for nIRFD and densitometry (TP1), respectively), which is determined by gel size and proximity to the camera, as well
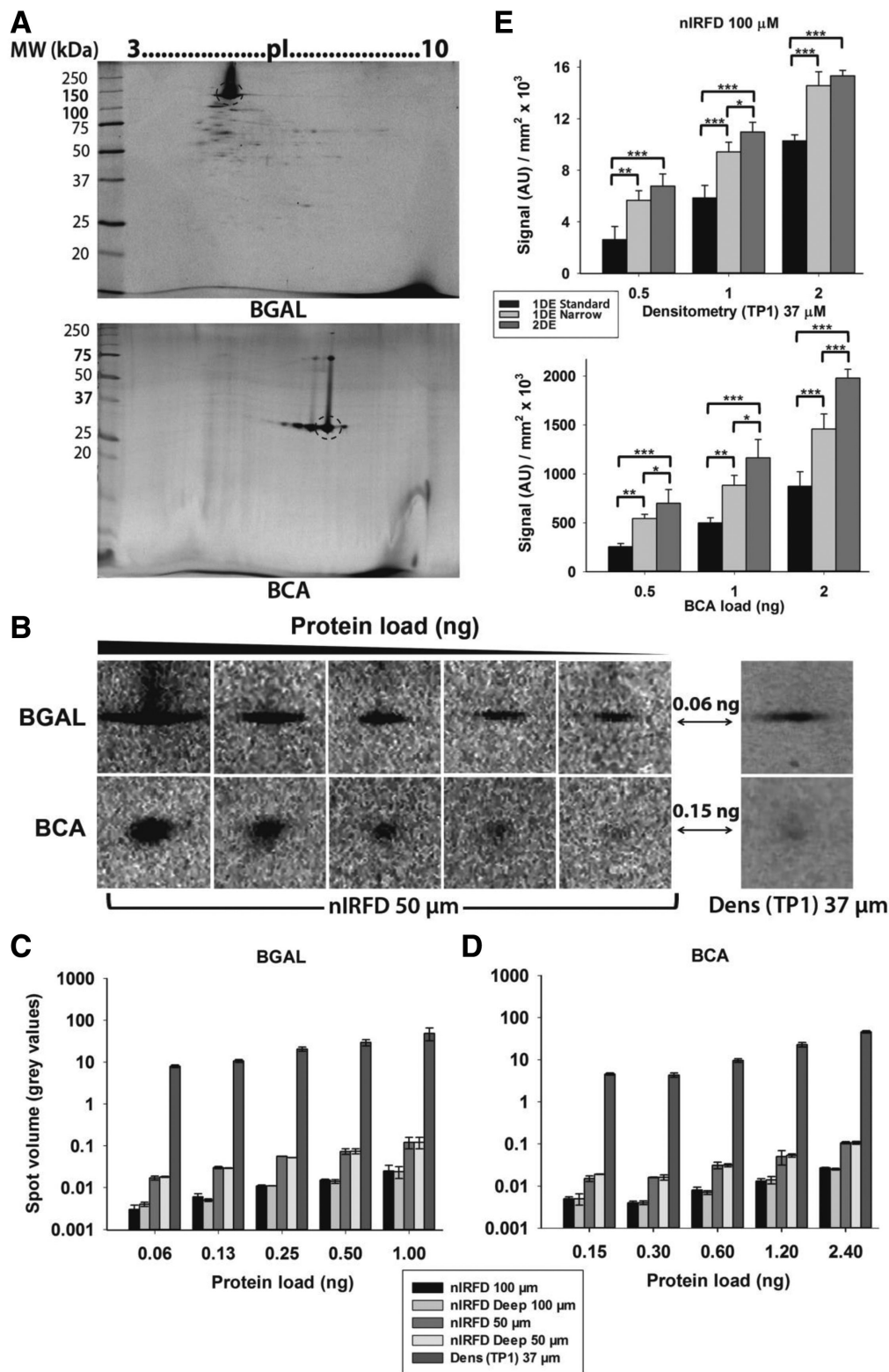
Figure 3. (A) Representative whole gel images following 2DE of 2 μg protein monomer loads of BGAL and BCA, imaged via 100 μm nIRFD; and (B) representative gel images showing target proteoforms following 2DE of 0.06–1 ng loads of BGAL, and 0.15–2.4 ng loads of BCA, imaged via 50 μm nIRFD. 37 μm densitometry images are shown for the lowest protein loads. For representative visualisation and comparison, images were contrasted to their maximum and minimum grey values. Bar graphs show spot volumes (grey values) derived from Delta2D analysis of whole and Deep images of 2DE-resolved (C) BGAL and (D) BCA (*n* = 3–4). (E) Bar graphs showing average background-subtracted 1DE band signal/mm² compared to that of 2DE spots following Multi Gauge analysis of standard-well and narrow-well 1DE of 0.5, 1, and 2 ng BCA, imaged via 100 μm nIRFD and 37 μm densitometry. Statistically significant differences (Post-hoc Holm-Šídák test) are indicated by '*', where one symbol indicates *p* < 0.05; two indicates *p* < 0.005; and three indicates *p* < 0.001 (One-way ANOVA, *p* < 0.001; *n* = 3–4).

as CCD pixel size (11 μm) and number (3.2 MP). However, lower resolution densitometry (i.e. lower TP) did not result in poorer LLD, despite S/N being reduced in a linear fashion with decreased resolution; nor was near-equivalent DS achieved with comparable 50 μm nIRFD and 49 μm densitometry (TP2), (Fig. 1B–F; Fig. 2B). Thus, rather than higher image resolution, the high 1DE DS with densitometry may be better explained by the nature of the imaging method and

CBB binding characteristics, as well as by the NaCl destain utilised.

It has been suggested that multiple CBB molecules may bind at a given site and/or form CBB 'stacks' [58, 59], with such structures likely minimally fluorescent, as is the case with unbound CBB molecules [19]. While nIRFD presumably detects only protein-bound CBB, densitometry (absorbance) would not discriminate between protein, self, or gel matrix-bound CBB (or potential light absorbing contaminants that might be present in gel, stain, and protein preparations), evidently resulting in comparatively higher intensity signal. As background staining was minimised by implementing the NaCl destain protocol [13], this likely facilitated the exceptionally high S/N (Fig. 2B). Indeed, protein signals (grey values, with black = 1) following 37 μm densitometry of 1DE- and 2DE-resolved standards were at least hundredfold higher compared with nIRFD (Fig. 3C–E), i.e. regions of interest were comprised of many more 'saturated'/black pixels. The same phenomenon was observed following quantitation of various spots following native proteome 2DE and 72 μm densitometry (TP4) versus nIRFD (not shown).

Nonetheless, despite exceptionally high DS following 1DE and 2DE of protein standards (Fig. 1B–F; Fig. 2; Fig. 3B–E), and that qualitative comparisons of 2DE gel images showed no marked variances in proteome coverage (Fig. 4), Delta2D analysis of the 2DE-resolved native proteome detected densitometrically resulted in spot counts only comparable to first-pass 100 μm nIRFD. Spot counts were 976 ± 118 and 989 ± 102, and fused image spot counts were 790 and 887, for 100 μm nIRFD and 37 μm densitometry, respectively (Fig. 5A and B). Both imaging conditions yielded comparable spot patterns, though examples of differences are shown (Fig. 5C). In general, smeared/streaked (i.e. poorly resolved) and relatively faint spots were better detected from 100 μm nIRFD images (Fig. 5C, A1, A6, A7, A9). Relatively small, well-resolved spots seemed better detected from 37 μm densitometry images (Fig. 5C A3, A8).

Using essentially equivalent imaging instrumentation as in this report, a recent study comparing fluorescence DS following 2D-DIGE concluded that the CCD/camera system offered comparable sensitivity to the laser/PMT system, though a tendency for improved spot detection patterns from laser/PMT-digitised images was noted [57]. The comparatively poor image resolution of the CCD/camera images was thought to account for the poorer 2DE DS (note that while camera resolution was 3.2 MP, large-format gels were analysed). In the present study, however, spot counts following 72 μm densitometry were not significantly different compared to 37 μm densitometry (1132 ± 71, and 910 for the fused image), confirming that densitometry image resolution did not significantly impact DS. Nonetheless, examples of apparently improved spot detection (Fig. 5C A2, A4, A8) and poorer spot detection (Fig. 5C A3, A7) are noted. The data thus suggest that the densitometry (CCD/camera-digitised) images were not processed by Delta2D in the same way as nIRFD images, perhaps due to the nature of the stored data
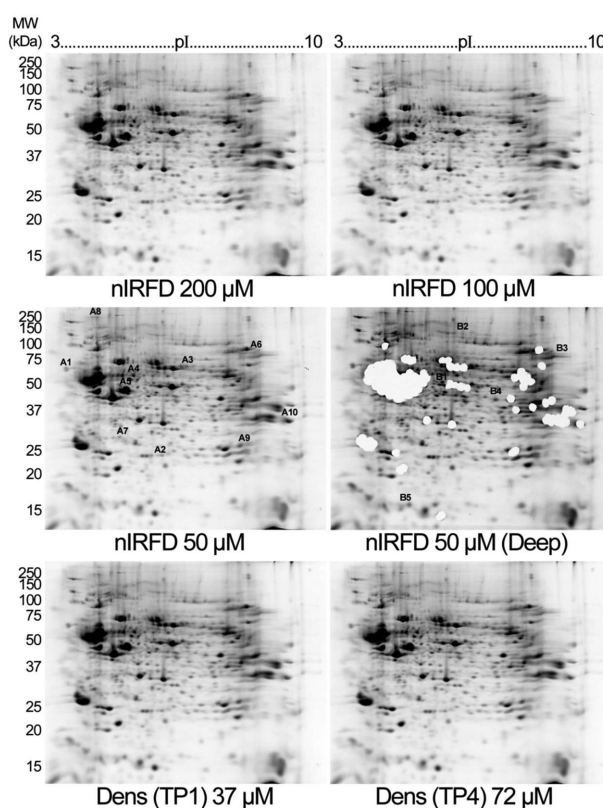

Figure 4. Representative 2DE gel images of cCBB-stained rat cortex soluble proteome (100 μg protein) following 200, 100, and 50 μm (600 V PMT) nIRFD, and 37 and 72 μm densitometry. A representative image of 50 μm (600 V PMT) nIRFD Deep Imaging is also shown. 50 μm nIRFD images are annotated with spot numbers corresponding to those shown in Figure 5C. For representative visualisation and comparison, images were contrasted to their maximum and minimum grey values.

(i.e. logarithmic versus linear conversion for the laser/PMT and CCD/camera system, respectively [50]).

Interestingly, it has been shown that the performance of Delta2D improves with increased noise [51]. nIRFD images processed in Delta2D presented granular residual backgrounds to a greater extent than 37 μm densitometry images following automated background subtraction, corroborating that nIRFD-imaged gel backgrounds were measurably less uniform (i.e. comparatively 'noisier'). Certainly, densitometry achieved substantially higher S/N compared to nIRFD (Fig. 2B; Fig. 3C–E), further suggesting software-related bias in favour of the lower S/N nIRFD images. Clearly, further investigation into the influence of 2DE analysis software and DS outcomes is required.

3.4 nIRFD resolution affects DS

Since quantitative analysis relies on the conversion and preservation of analogue data (i.e. the stained physical gel and resolved proteins within) to digital data (i.e. image acquisition), higher information/resolution images are expected
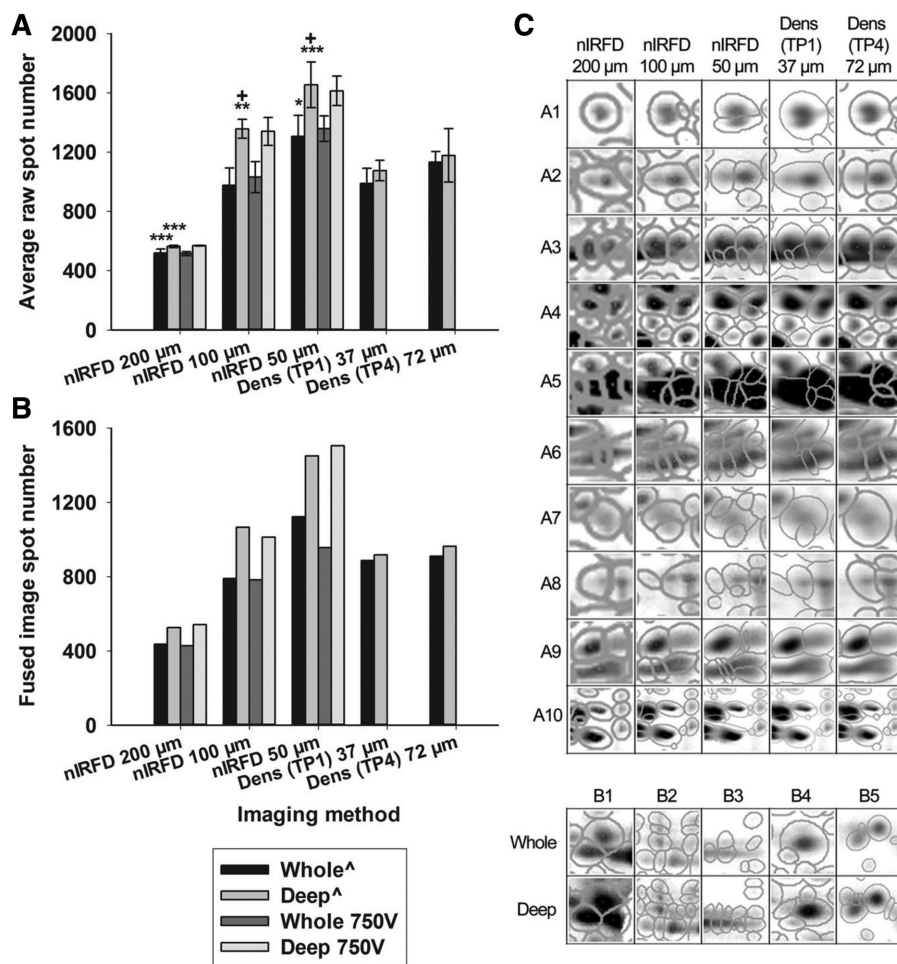
Figure 5. Delta2D spot counts from (A) raw and (B) fused 2DE gel images following whole and Deep Imaging with 200, 100, and 50 μm nIRFD (600 V (ˆ) and 750 V PMT), and 37 and 72 μm densitometry. Statistically significant differences (Student's *t*-test) from whole versus Deep Imaged gels are indicated by '+'. Statistically significant differences (Post-hoc Holm-Šídák test) from 100 μm 600 V PMT nIRFD are indicated by '*'. One symbol indicates $p < 0.05$; two indicates $p < 0.005$; and three indicates $p < 0.001$ (One-way ANOVA, $p < 0.001$; $n = 3$). (C) Select regions of analysed raw images of a single replicate, which exemplify differences in spot detection patterns following varied methods of whole gel imaging (A1–10) and 50 μm (600 V PMT) Deep Imaging (B1–5), are shown.

to improve analyses and facilitate greater DS [17, 34, 35]. For both 1DE and 2DE, higher resolution imaging should mean more defined band or spot boundaries, more detailed and accurate capture of grey levels across the gel, and potentially increased signal from a given region due to increased pixel number. For fluorescence imaging, reduced sensitivity with increased resolution / reduced pixel size is expected [50]. For 2DE, improved resolution should also enhance the ability of a given analysis tool – be it the naked eye or analysis software – to distinguish between two or more closely positioned or overlapping spots. Here, the impact of image resolution on 1DE and 2DE DS was assessed following 200, 100, and 50 μm-pixel nIRFD using the FLA 9000 (laser/PMT system), for which pixel size refers to scanning step size.

In theory, reduced nIRFD resolution should have resulted in comparatively higher S/N and thus overall higher DS since more light emissions are able to reach the PMT with larger pixel size [50]. Based on this rationale, 200 μm-pixel laser/PMT imaging using similar Typhoon imagers has commonly been used in 2D-DIGE analyses, presumably in an attempt to maximise sensitivity as recommended in the Typhoon User's Guide v.3.0 (Amersham Biosciences / GE Healthcare, Buckinghamshire, UK), though seemingly with-

out consideration for the impacts of low image resolution on software-dependent analysis outcomes. For instance, studies have used 200 μm imaging followed by analyses with DeCyder™ (GE Healthcare, Buckinghamshire, UK) [52, 53], the user guide(s) of which explicitly stipulate that images with no smaller than 100 μm pixels should be subject to analysis (https://www.gelifesciences.com).

The data here show that 200 μm nIRFD resulted in the poorest S/N (Fig. 2B) and equal or significantly poorer LLD with generally higher variability (Fig. 1B–F). While IMPS values suggested that one may 'make do' with lower resolution nIRFD imaging for sufficient 2DE DS at least in terms of LLD (Fig. 2A), only ~50% of the protein spots detected from 100 μm nIRFD images were detected from 200 μm images following Delta2D analysis of the 2DE-resolved native proteome. Spot counts were 519 ± 26 and 436 from the fused image (Fig. 5A and B), marking a significant decrease in 2DE DS with lower resolution nIRFD. Examination of spot detection patterns revealed more frequent incidences of missed spots and inaccurate spot boundaries (Fig. 5C). Many low-abundance spots were indistinguishable from, and presumably automatically subtracted along with gel background, and thus were not detected (Fig. 5C A1, A4, A6); and poorly resolved

proteoforms were generally indistinguishable from each other and grouped within single boundaries (Fig. 5C, A5–7, A9).

It is possible that the measured decrease in 1DE S/N with 200 μm nIRFD may in part be attributed to the stain utilised, consistent with some signal from stained matrix despite the expectation that primarily only protein-bound CBB should fluoresce [16, 19]. Again, however, evidence suggests that poor S/N would not have so negatively impacted Delta2D analysis [51], indicating that low image resolution was the primary cause of the decreased 2DE DS observed. Certainly, the Delta2D imaging guide (https://www.decodon.com) highlights the need for adequate image resolution for optimal analysis outcomes. Thus, laser/PMT imaging resolution should not be compromised if one wishes to maximise the comprehensiveness of quantitative gel-based comparative proteomics, which ultimately relies on the performance of 2DE analysis software. The potential for improvements to DS with high imaging resolution are exemplified by results following 50 μm nIRFD.

1DE DS measurements following 50 μm nIRFD were practically identical to those obtained following standard 100 μm nIRFD (Fig. 1B–F; Fig. 2A and B) initially suggesting that 100 μm nIRFD offered sufficiently high image resolution for optimal DS. However, DS for the 2DE-resolved native proteome was substantially improved with 50 μm nIRFD, evident not only by increased spot counts (1306 $\pm$ 141, and 1123 for the fused image (Fig. 5A and B)), but by improved spot detection patterns (Fig. 5A–C). With few exceptions (Fig. 5C, A10), 50 μm nIRFD resulted in better 'splitting' of spots, i.e. spot boundaries of overlapping proteoforms were determined with greater accuracy. Note, that 2DE of individual protein standards confirmed that 100 and 50 μm nIRFD achieved the same LLD, as determined from 1DE DS assessments (Fig. 1B–F; Fig. 2A; Fig. 3B–D). However, 2DE spot volumes were increased with 50 μm nIRFD (Fig. 3C and D), i.e. 2DE S/N was improved with increased nIRFD resolution. Significantly higher S/N with 50 μm nIRFD was not observed following 1DE analysis (Fig. 2B), and such inconsistencies again highlight that analysis methods (e.g. the software utilised, the ways in which background values are determined and subtracted, and so forth) play a major role in DS outcomes [54]. A quantitative analysis approach that can be applied equally well to both 1DE and 2DE gel images may be instrumental to definitively characterising DS, thus exploring the capabilities of other available image analysis packages is worthwhile in this regard. Briefly, although reasonable attempts were made to quantitatively analyse 1DE gels using Delta2D, this was ultimately unsuccessful due to limitations in defining regions of interest. At most, qualitative assessments suggested that 1DE DS with Delta2D versus Multi Gauge would perhaps be higher, as low protein loads were more visually apparent in Delta2D for both nIRFD and densitometry images (not shown).

In addition to increased spot counts from 50 μm nIRFD images, Delta2D automated image warping (i.e. a process to align gel images) was more accurate than when performed with lower resolution images, with frequency and accuracy of matched warping vectors decreasing with decreased resolution / increased pixel size (not shown). Improved alignment accuracy with higher resolution nIRFD minimised the need for manual intervention, and very likely contributed to the improved spot detection observed. As image analysis is universally regarded as the 'bottleneck' for larger scale gel-based proteomic investigations [55], improving 2DE analysis accuracy and outcomes while reducing overall processing time is particularly advantageous. While these advantages come at the cost of additional imaging time and increased file size, these data demonstrate that such compromises are more worthwhile, and less problematic with current computing and storage capacities, than typically suggested in the past. Notably, the FLA 9000 is also capable of 25 μm scanning, though scan time was excessive and resulted in considerable drying and distortion of gels despite attempts to maintain hydration. Preliminary findings were that native proteome 2DE DS decreased to that of 100 μm nIRFD despite visibly improved image quality (not shown), indicating that it is the balance between high quality input and the capacity of analysis software to maximise output that, in part, underlies improvements to DS.

3.5 Deep Imaging improves 2DE DS

Fluorescence Deep Imaging of SR-stained 2DE gels improves proteome coverage, achieved by increasing signal from low-abundance proteoforms following the removal of saturated gel regions and reimaging [3, 4, 56]. Here, we aimed to quantify the DS of cCBB nIRFD Deep Imaging from narrow-well 1DE models, and maximise 2DE DS by coupling Deep Imaging with the nIRFD imaging conditions assessed.

Deep Imaging of narrow-well 1DE models did not result in improved LLD or S/N compared with first-pass whole gel imaging (not shown). However, following nIRFD Deep Imaging of the 2DE-resolved proteome, Delta2D-derived spot counts were significantly increased, by $\geq$ ~30% relative to first-pass imaging (Fig. 5A and B). For 200 μM nIRFD, spot count increased to 563 $\pm$ 8 (525 from the fused image, i.e. 88 additional spots); for 100 μm nIRFD, spot count increased to 1357 $\pm$ 63 (1066 spots from the fused image, i.e. 276 additional spots); and for 50 μm nIRFD, spot count increased to 1654 $\pm$ 154 (1449 from the fused image, i.e. 326 additional spots). Examination of spot detection patterns revealed that conjoined or otherwise poorly resolved spots were better defined and detected, particularly when coupled with 50 μm nIRFD (Fig. 5C and B1–5).

Notably, spot counts from both whole and Deep imaged gels were unchanged using 750 V versus 600 V PMT (Fig. 5A and B), and quantification of 2DE-resolved protein standards showed that spot volumes were not increased following Deep Imaging with 750 V PMT (Fig. 3C and D). Taken together, these results suggest that the increased 2DE DS observed here following native proteome Deep Imaging was not attributable

to the fluorescence integration observed previously with SR staining and CCD/camera nIRFD [4], likely due to a finite opportunity for signal integration, i.e. excitation/dwell time cannot be increased with the laser/PMT imager. Indeed, the data instead suggest that the benefits of cCBB nIRFD Deep Imaging using the FLA-9000 imaging system were largely a result of Delta2D image analysis, perhaps being a favourable consequence of the resulting narrower range of grey levels following excision of saturated regions. One might therefore expect that densitometry 'Deep Imaging' would result in similar improvements to DS, though no significant improvements were observed. 1075 ± 68 and 1178 ± 180 spots were detected, and 917 and 963 spots (i.e. an additional 30 and 53 spots) were detected from fused images, following 37 and 72 μm densitometry, respectively (Fig. 5A and B). This is likely explained by the comparatively immense spot volumes from densitometry images (Fig. 3C–E; Fig. 5A and B) indicating that image dynamic range would be minimally impacted following excision of saturating gel regions.

Accepting that improvements seen here with Deep Imaging were in fact predominantly or purely attributed to the performance of the analysis software, 2DE DS of cCBB nIRFD with a laser/PMT system would thus heavily depend on the dynamic range of proteins within a sample. Multiple rounds of high-resolution nIRFD Deep Imaging may be necessary to maximally 'mine' a given resolved proteome. The use of a CCD/camera imaging systems for nIRFD should enable full capitalisation of Deep Imaging based on genuine integration of fluorescence signals [4], provided instrument sensitivity is adequate and resulting images can be optimally analysed. However, such instrumentation, which generally utilise lamps and LEDs rather than lasers, may be expected to be less sensitive (depending on the fluorophore used) due to broader wavelength excitation and emission hardware. Due focus should continue to be placed on improving imaging and analysis approaches in order to maximise outcomes of proteomic investigations, as recently demonstrated by a number of groups [48, 51, 54]. It is clear that the capacity for proteome coverage and detection using 2DE and cCBB staining (and thus likely many other stains) has in general been grossly underestimated [3, 8, 13, 15].

4 Concluding remarks

Measuring DS from narrow-well 1DE models utilising commercial standards independently assessed for concentration and purity indicates that the modified cCBB staining/destaining protocol described by Gauci et al. [13] achieves low- to sub-femtomole DS for intact 1DE- and 2DE-resolved protein standards, detected with either nIRFD or densitometry. The data show that cCBB DS for intact proteins/proteoforms rivals that of current peptide DS in Bottom-up MS analytical approaches [60,61]. This is clearly of substantial benefit in terms of Discovery Proteomics (e.g. analysing molecular mechanisms and identifying critical biomarkers), and should thus also enable and promote genuine complementary application of both Top-down and Bottom-up proteomic approaches.

DS following densitometric detection of the cCBB-stained native proteome was comparable to that of first-pass 100 μm nIRFD, providing simple, cost-effective access to high sensitivity Top-down proteomics. Improved or alternative 2DE image analysis software than utilised here may further optimise 2DE DS with densitometry. Higher resolution nIRFD improved the process and outcomes of 2DE analysis, enabling more accurate automated image warping and increased spot detection, further still with nIRFD Deep Imaging – although the increased 2DE DS seemed linked to the performance of image analysis software rather than genuine fluorescence integration. Overall, this study highlights the importance of considering factors other than the stain itself that can influence DS, and will hopefully prompt the proteomics community to develop standard protocols to assess DS.

The authors have declared no conflict of interest.

5 References

[1] Butt, R. H., Coorssen, J. R., *J. Proteome Res.* 2006, *5*, 437–448.

[2] Butt, R. H., Coorssen, J. R., *J. Proteome Res.* 2005, *4*, 982–991.

[3] Wright, E. P., Partridge, M. A., Padula, M. P., Gauci, V. J., Malladi, C. S., Coorssen, J. R, *Proteomics* 2014, *14*, 872–889.

[4] Wright, E. P., Prasad, K. A., Padula, M. P., Coorssen, J. R., *PLoS One* 2014, *9*, e86058.

[5] Miller, I., Eberini, I., Gianazza, E., *Proteomics* 2010, *10*, 586–610.

[6] Rogowska-Wrzesinska, A., Le Bihan, M. C., Thaysen-Andersen, M., Roepstorff, P., *J. Proteomics* 2013, *88*, 4–13.

[7] Wittmann-Liebold, B., Graack, H. R., Pohl, T., *Proteomics* 2006, *6*, 4688–4703.

[8] Oliveira, B. M., Coorssen, J. R., Martins-De-Souza, D., *J. Proteomics* 2014, *104*, 140–150.

[9] Coorssen, J., Yergey, A., *Proteomes* 2015, *3*, 440–453.

[10] Magdeldin, S., Enany, S., Yoshida, Y., Xu, B., Zhang, Y., Zureena, Z, Lokamani, I., Yaoita, E., Yamamoto, T., *Clin. Proteomics* 2014, *11*, 1–10.

[11] Jungblut, J. R., Holzhütter, H. G., Apweiler, R., Schlüter, H., *Chem. Cent. J.*, 2008, *2*, 16.

[12] Thiede, B., Koehler, C. J., Strozynski, M., Treumann, A., Stein, R., Zimny-Arndt, U., Schmid, M., Jungblut, P. R., *Mol. Cell. Proteomics* 2013, *12*, 529–538.

[13] Gauci, V. J., Padula, M. P., Coorssen, J. R., *J. Proteomics* 2013, *90*, 96–106.

[14] Gauci, V. J., Wright, E. P., Coorssen, J. R., *J.Chem. Biol.* 2011, *4*, 3–29.

[15] Butt, R. H., Coorssen, J. R., *Mol. Cell. Proteomics* 2013, *12*, 3834–3850.

[16] Harris, L. R., Churchward, M. A., Butt, R. H., Coorssen, J. R., *J. Proteome Res.* 2007, *6*, 1418–1425.

[17] Patton, W. F., *J.Chromatogr. A* 1995, *689*, 55–87.

[18] Coorssen, J. R., Blank, P. S., Albertorio, F., Bezrukov, L., Kolosova, I., Backlund, P. S., Zimmerberg, J., *Anal. Biochem.* 2002, *307*, 54–62.

[19] Luo, S., Wehr, N. B., Levine, R. L., *Anal. Biochem.* 2006, *350*, 233–238.

[20] Szule, J. A., Jarvis, S. E., Hibbert, J. E., Spafford, J. D., Braun, J. E., Zamponi, G. W., Wessel, G. M., Coorssen, J. R., *J.Biol. Chem.* 2003, *278*, 24251–24254.

[21] Neuhoff, V., Arold, N., Taube, D., Ehrhardt, W., *Electrophoresis* 1988, *9*, 255–262.

[22] Neuhoff, V., Stamm, R., Eibl, H., *Electrophoresis* 1985, *6*, 427–448.

[23] Kang, D., Gho, Y. S., Suh, M., Kang, C., *Bull. Korean Chem. Soc.* 2002, *23*, 1511–1512.

[24] Choi, J. K., Chae, H. Z., Hwang, S. Y., Choi, H. I., Jin, L. T., Yoo, G. S., *Electrophoresis* 2004, *25*, 1136–1141.

[25] Candiano, G., Bruschi, M., Musante, L., Santucci, L., Ghiggeri, G. M., Carnemolla, B., Orecchia, P., Zardi, L., Righetti, P. G., *Electrophoresis* 2004, *25*, 1327–1333.

[26] Winkler, C., Denker, K., Wortelkamp, S., Sickmann, A., *Electrophoresis* 2007, *28*, 2095–2099.

[27] Dong, W., Wang, T., Wang, F., Zhang, J., *PloS One* 2011, *6*, e22394.

[28] Lin, J. F., Chen, Q. X., Tian, H. Y., Gao, X., Yu, M. L., Xu, G. J., Zhao, F. K., *Anal. Bioanal. Chem.* 2008, *390*, 1765–1773.

[29] Chevalier, F., Rofidal, V., Vanova, P., Bergoin, A., Rossignol, M., *Phytochemistry* 2004, *65*, 1499–1506.

[30] Smejkal, G. B., Robinson, M. H., Lazarev, A., *Electrophoresis* 2004, *25*, 2511–2519.

[31] Berggren, K. N., Schulenberg, B., Lopez, M. F., Steinberg, T. H., Bogdanova, A., Smejkal, G., Wang, A., Patton, W. F., *Proteomics* 2002, *2*, 486–498.

[32] Steinberg, T. H., Haugland, R. P., Singer, V. L., *Anal. Biochem.* 1996, *239*, 238–245.

[33] Steinberg, T. H., Jones, L. J., Haugland, R. P., Singer, V. L., *Anal. Biochem.* 1996, *239*, 223–237.

[34] Patton, W. F., *Electrophoresis* 2002, *21*, 1123–1144.

[35] Née, M., Gauci, V. J., Noaman, N., Coorssen, J. R., *eLS* 2016, 1–10.

[36] Coorssen, J. R., Blank, P. S., Albertorio, F., Bezrukov, L., Kolosova, I., Chen, X., Backlund, P. S., Zimmerberg, J., *J.Cell. Sci.* 2003, *116*, 2087–2097.

[37] Cannon-Carlson, S., Tang, J., *Anal. Biochem.* 1997, *246*, 148–150.

[38] Laemmli, U. K., *Nature*, 1970, *227*, 680–685.

[39] Grimsley, G. R., Pace, C. N., *Curr. Protoc. Protein Sci.* 2004, *33*, 3.1.1–3.1.9.

[40] Churchward, M. A., Butt, R. H., Lang, J. C., Hsu, K. K., Coorssen, J. R., *Proteome Sci.* 2005, *3*, 5.

[41] Butt, R. H., Pfeifer, T. A., Delaney, A., Grigliatti, T. A., Tetzlaff, W. G., Coorssen, J. R., *Mol. Cell. Proteomics* 2007, *6*, 1574–1588.

[42] Long, G. L., Windefordner, J. D., *Anal. Chem.* 1983, *55*, 712–724.

[43] Sidak, Z., *J. Am. Stat. Assoc.* 1967, *62*, 626–633.

[44] Tal, M., Silberstein, A., Nusser, E., *J. Biol. Chem.* 1985, *260*, 9976–9980.

[45] Wang, X., Li, X., Li, Y., *Biotechnol. Lett.* 2007, *29*, 1599–1603.

[46] Choi, J.-K., Yoon, S.-H., Hong, H.-Y., Choi, D.-K., Yoo, G.-S., *Anal. Biochem.* 1996, *236*, 82–84.

[47] Pink, M., Verma, N., Rettenmeier, A. W., Schmitz-Spanke, S., *Electrophoresis* 2010, *31*, 593–598.

[48] Sandberg, A., Buschmann, V., Kapusta, P., Erdmann, R., Wheelock, A. M., *Anal. Chem.* 2016, *88*, 3067–3074.

[49] Neuhoff, V., Stamm, R., Pardowitz, I., Arold, N., Ehrhardt, W., Taube, D., *Electrophoresis* 1990, *11*, 101–117.

[50] Miura, K., *Proteomics* 2003, *3*, 1097–1108.

[51] Sengar, R. S., Upadhyay, A. K., Singh, M., Gadre, V. M., *Biomed. Signal Process Control* 2016, *25*, 62–75.

[52] Serra-Soriano, M., Navarro, J. A., Genoves, A., Pallas, V., *J. Proteomics*, 2015, *124*, 11–24.

[53] Lincet, H., Guevel, B., Pineau, C., Allouche, S., Lemoisson, E., Poulain, L., Gauduchon, P., *J. Proteomics* 2012, *75*, 1157–1169.

[54] Stessl, M., Noe, C. R., Lachmann, B., *Electrophoresis* 2009, *30*, 325–328.

[55] Clark, B. N., Gutstein, H. B., *Proteomics*, 2008, *8*, 1197–1203.

[56] Partridge, M. A., Gopinath, S., Myers, S. J., Coorssen, J. R., *J. Chem. Biol.* 2016, *9*, 9–18.

[57] Strijkstra, A., Trautwein, K., Roesler, S., Feenders, C., Danzer, D., Riemenschneider, U., Blasius, B., Rabus, R., *Proteomics* 2016, *16*, 1975–1979.

[58] Congdon, R. W., Muth, G. W., Splittgerber, A. G., *Anal. Biochem.* 1993, *213*, 407–413.

[59] Wilson, C.M., *Anal. Biochem.* 1979, *96*, 263–278.

[60] Hawkridge, A.M., *Practical Considerations and Current Limitations in Quantitative Mass Spectrometry-based Proteomics*, The Royal Society of Chemistry, United Kingdom 2014, pp. 1–25.

[61] Thakur, S. S., Geiger, T., Chatterjee, B., Bandilla, P., Fröhlich, F., Cox, J., Mann, M., *Mol. Cell. Proteomics* 2011, *10*, M110.003699.